In vivo imaging of hydrogen peroxide with chemiluminescent nanoparticles

DONGWON LEE[1]*, SIRAJUD KHAJA[1]*, JUAN C. VELASQUEZ-CASTANO[2], MADHURI DASARI[1], CARRIE SUN[3], JOHN PETROS[3,4], W. ROBERT TAYLOR[1,2,4] AND NIREN MURTHY[1†]

[1]The Wallace H. Coulter Department of Biomedical Engineering and Parker H. Petit Institute for Bioengineering and Bioscience, Georgia Institute of Technology, Atlanta, Georgia 30332, USA

[2]Cardiology Division, Department of Medicine, Emory University School of Medicine, Atlanta, Georgia 30322, USA

[3]Department of Urology, Emory University School of Medicine, Atlanta, Georgia 30322, USA

[4]The Atlanta VA Medical Center, Decatur, Georgia 30033, USA

*These authors contributed equally to this work

[†]e-mail: niren.murthy@bme.gatech.edu

Published online: 19 August 2007; doi:10.1038/nmat1983

The overproduction of hydrogen peroxide is implicated in the development of numerous diseases[1–4] and there is currently great interest in developing contrast agents that can image hydrogen peroxide *in vivo*. In this report, we demonstrate that nanoparticles formulated from peroxalate esters and fluorescent dyes can image hydrogen peroxide *in vivo* with high specificity and sensitivity. The peroxalate nanoparticles image hydrogen peroxide by undergoing a three-component chemiluminescent reaction between hydrogen peroxide, peroxalate esters and fluorescent dyes. The peroxalate nanoparticles have several attractive properties for *in vivo* imaging, such as tunable wavelength emission (460–630 nm), nanomolar sensitivity for hydrogen peroxide and excellent specificity for hydrogen peroxide over other reactive oxygen species. The peroxalate nanoparticles were capable of imaging hydrogen peroxide in the peritoneal cavity of mice during a lipopolysaccharide-induced inflammatory response. We anticipate numerous applications of peroxalate nanoparticles for *in vivo* imaging of hydrogen peroxide, given their high specificity and sensitivity and deep-tissue-imaging capability.

The development of contrast agents that can image hydrogen peroxide *in vivo* remains a major challenge in the field of molecular imaging. Imaging hydrogen peroxide *in vivo* has been difficult because of its low concentration and low reactivity in comparison with other reactive oxygen species. At present, fluorescent probes based on boronates are the only contrast agents that can detect hydrogen peroxide at physiologic concentrations with high specificity[2–7]; however, their potential for *in vivo* imaging is limited because of low tissue penetration[8,9].

In this letter we present for the first time a contrast agent that can image hydrogen peroxide *in vivo*[10], with high specificity and sensitivity[11], termed peroxalate nanoparticles. The peroxalate nanoparticles image hydrogen peroxide by carrying out a three-component chemiluminescent reaction between hydrogen peroxide, peroxalate esters and fluorescent dyes. The details of this strategy are shown in Fig. 1. Compound **1** forms the scaffold of the peroxalate nanoparticles and is a hydrophobic polymer that contains peroxalate esters in its backbone. The peroxalate nanoparticles (**3**) are formulated from **1** and fluorescent dye (**2**), generating nanoparticles that have fluorescent dyes surrounded by peroxalate esters. The peroxalate nanoparticles image hydrogen peroxide through a two-step process. First, hydrogen peroxide diffuses into the nanoparticles and reacts with the peroxalate ester groups, generating a high-energy dioxetanedione within the nanoparticles[12–18]. This dioxetanedione then chemically excites encapsulated fluorescent dyes (**4**), through the chemically initiated electron-exchange luminescence mechanism[13,19–21], leading to chemiluminescence from the nanoparticles (**5**) and the imaging of hydrogen peroxide.

Polymer **1** was synthesized through the reaction of hydroxybenzyl alcohol, octanediol and oxalyl chloride, and was chosen for imaging studies because it possesses an optimal trade-off between stability in aqueous environments and reactivity to hydrogen peroxide (see the Supplementary Information). Initial hydrogen peroxide chemiluminescence experiments were carried out with the fluorescent dye rubrene. Nanoparticles formulated from **1** and rubrene had a mean size of 550 nm, as determined by dynamic light scattering. The chemiluminescence from these nanoparticles in the presence of varying concentrations of hydrogen peroxide was investigated. Figure 2a demonstrates that nanoparticles composed of **1** and rubrene chemiluminesce in the presence of hydrogen peroxide and also have a linear correlation between hydrogen peroxide concentration and chemiluminescence intensity, within the concentration range of 0–10 μM. The peroxalate nanoparticles were also capable of detecting hydrogen peroxide at concentrations as low as 250 nM (Fig. 2b), and thus can detect hydrogen peroxide at physiologically relevant concentrations. The peroxalate nanoparticles have a 60:1 molar excess of peroxalate esters to fluorescent dyes. This excess of peroxalate esters should act as a continuous energy source, and enable the peroxalate nanoparticles to chemiluminesce for an extended period of time in the presence of hydrogen peroxide. We investigated the kinetics of chemiluminescence from the peroxalate nanoparticles in the presence of hydrogen peroxide. The chemiluminescence emission intensity has a half-life of approximately 25 min in the presence of 10 μM hydrogen peroxide, and should therefore be suitable for numerous *in vivo* imaging applications (see Supplementary Information, Fig. S5).

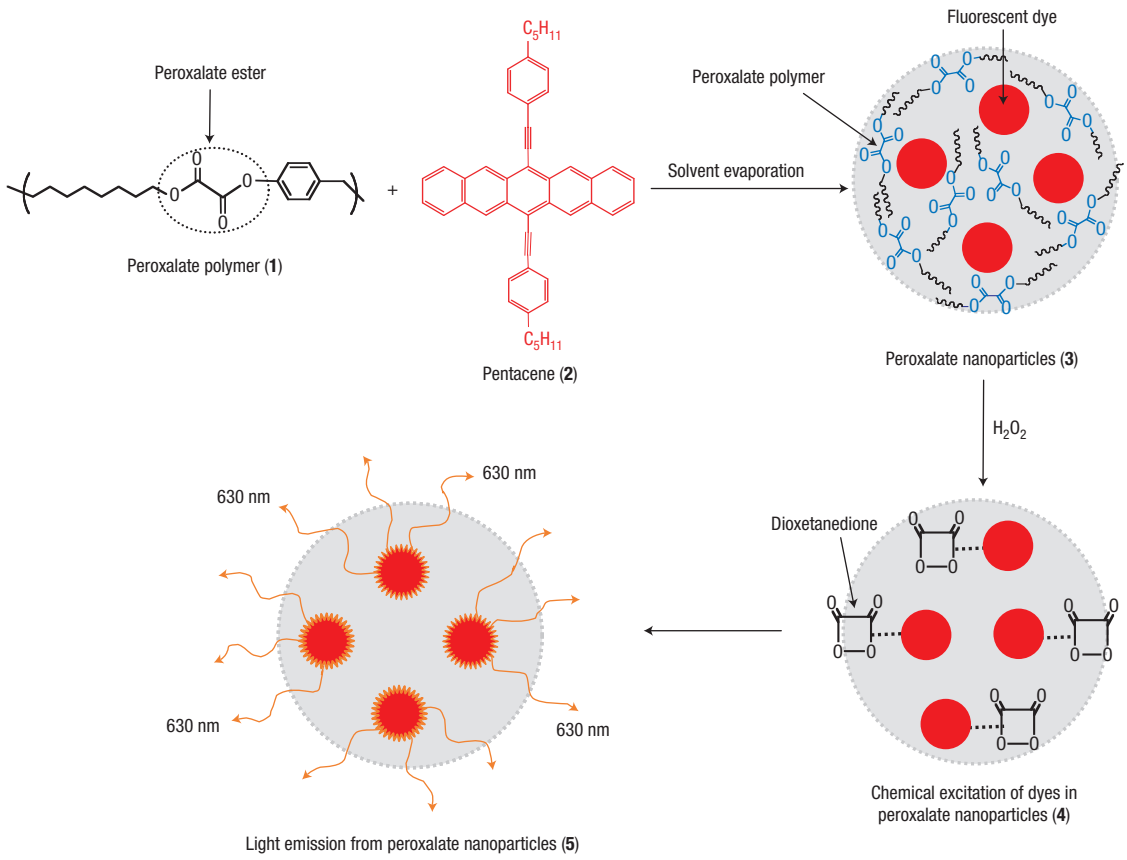

Figure 1 Peroxalate nanoparticles—a new strategy for imaging hydrogen peroxide *in vivo*. Peroxalate nanoparticles (**3**) are formulated from the peroxalate polymer (**1**) and a fluorescent dye (**2**), in this case pentacene. Hydrogen peroxide reacts with the peroxalate ester of **3** to produce a high-energy dioxetanedione intermediate within the nanoparticles (**4**), which then chemically excites the encapsulated dye, leading to light emission from the nanoparticles and the imaging of hydrogen peroxide (**5**).

A key advantage of using peroxalate nanoparticles for imaging hydrogen peroxide is their potential for generating chemiluminescence at high emission wavelengths. This is because the dioxetanedione intermediate produced within the nanoparticles can chemically excite a variety of fluorescent dyes[19], including those in the near-infrared range. Chemiluminescence emission wavelengths greater than 600 nm are ideally suitable for deep-tissue imaging (>1 cm) owing to the minimal absorption by haemoglobin, water and lipids at these wavelengths[9,22]. The wavelength tunability of the peroxalate nanoparticles was investigated by encapsulating rubrene, perylene and pentacene and measuring their emission spectra in the presence of hydrogen peroxide. Figure 2c shows that peroxalate particles containing perylene, rubrene and pentacene emitted light at wavelengths of 460, 560 and 630 nm, respectively, which are similar to the fluorescent emission wavelengths of these dyes. The chemiluminescence emission wavelength of peroxalate nanoparticles can therefore be tuned to high wavelengths by simply changing the fluorescent dye encapsulated within the nanoparticle. Peroxalate nanoparticles, therefore, have the potential for deep-tissue imaging of hydrogen peroxide.

Another appealing feature of peroxalate nanoparticles for imaging hydrogen peroxide is their specificity for hydrogen peroxide over other reactive oxygen species. Peroxalate chemiluminescence requires the generation of a four-membered dioxetanedione intermediate, which can be formed only by hydrogen peroxide, and not by other reactive oxygen species, such as superoxide or nitric oxide. The specificity of peroxalate nanoparticles containing rubrene to hydrogen peroxide was therefore investigated. Figure 2d shows that peroxalate nanoparticles have considerable selectivity for hydrogen peroxide over other reactive oxygen species. For example, at 10 μM hydrogen peroxide, peroxalate nanoparticles gave a chemiluminescent intensity of 1.3×10^6 RLU s^{-1}, which is 50 times higher than with either *tert*-butyl peroxide or the hydroxide radical. The superoxide anion generated ten times less chemiluminescence than hydrogen peroxide, but this value was mainly due to the spontaneous dismutation of superoxide into hydrogen peroxide, as shown by its inhibition in the presence of catalase, a hydrogen peroxide-scavenging enzyme.

The ability of the peroxalate nanoparticles containing pentacene to detect hydrogen peroxide in deep tissues of mice was investigated. Pentacene was chosen as a fluorescent dye for *in vivo* imaging because of its high emission wavelength (630 nm) and consequent high level of tissue penetration. First, to demonstrate the feasibility of deep-tissue imaging using peroxalate nanoparticles, a suspension of nanoparticles (300 μg) in the absence or presence of hydrogen peroxide (1 and 10 μM) was injected intramuscularly at a depth of ~3 mm and imaged in an IVIS imaging system. Figure 3 demonstrates that the peroxalate nanoparticles can detect exogenous hydrogen peroxide. For example, a peak emission intensity of 80,000 p s^{-1} cm^{-2} sr^{-1} was observed from the particles injected with 10 μM hydrogen peroxide (I), whereas a peak emission intensity of only 20,000 p s^{-1} cm^{-2} sr^{-1}

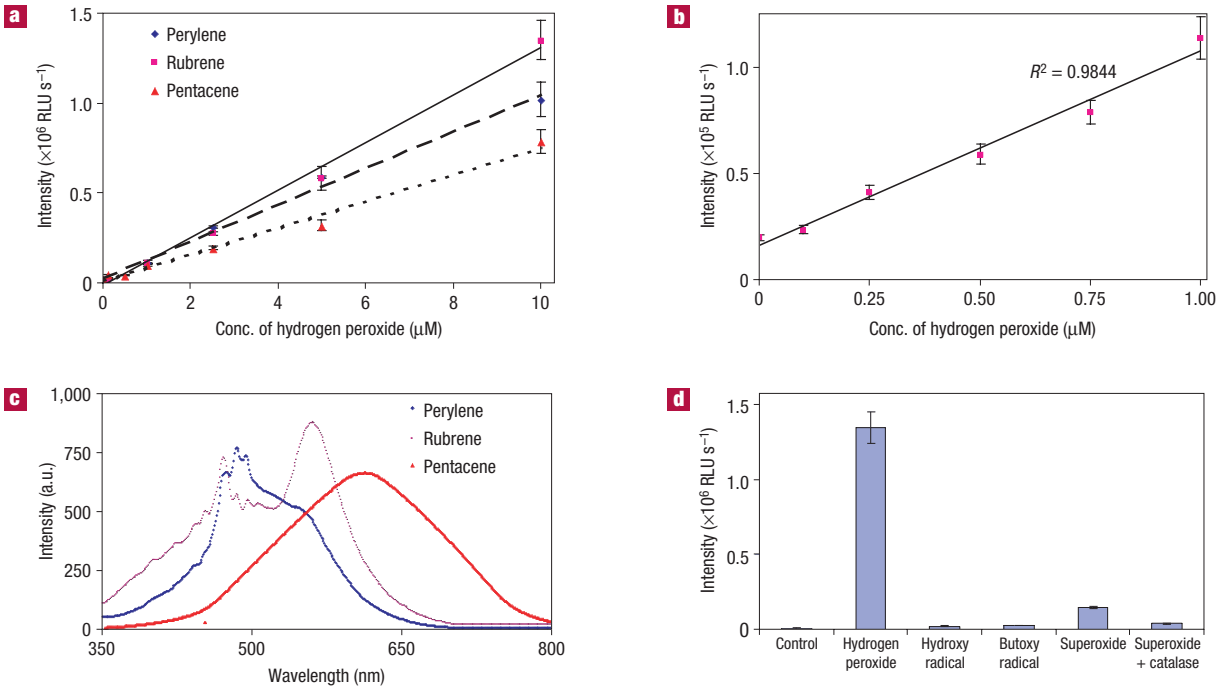

Figure 2 Peroxalate nanoparticles have high sensitivity and specificity for hydrogen peroxide, and also tunable emission wavelengths. a, Peroxalate nanoparticles show a linear correlation between chemiluminescence intensity and the concentration of hydrogen peroxide. Mean ± s.d., $n = 3$. Data shown are obtained from 1 mg of peroxalate nanoparticles in response to the addition of increasing concentrations of hydrogen peroxide. RLU, relative light units. **b**, Chemiluminescence intensity of rubrene-encapsulated nanoparticles at a concentration of hydrogen peroxide less than 1 μM. Mean ± s.d., $n = 3$. **c**, Chemiluminescent emission spectra of peroxalate nanoparticles, containing either perylene, rubrene or pentacene, in the presence of hydrogen peroxide. **d**, Chemiluminescence response of rubrene-loaded peroxalate nanoparticles (1 mg ml^{-1}) to various reactive oxygen species. Superoxide was added as solid KO_2. Hydroxyl radical and butoxy radical were generated by the reaction of 10 mM of Fe^{2+} with 1 mM hydrogen peroxide or 1 mM *tert*-butyl hydroperoxide. Mean ± s.d., $n = 3$.

was detected from particles injected with 1 μM hydrogen peroxide (II) and much lower emission was observed from the particles without hydrogen peroxide (III).

We also investigated the ability of the peroxalate nanoparticles to image endogenously produced hydrogen peroxide in mice. The overproduction of hydrogen peroxide is implicated in the development of numerous inflammatory diseases, such as atherosclerosis, chronic obstructive pulmonary disease and liver hepatitis[23–27]. Therefore, there is a great interest in imaging hydrogen peroxide *in vivo* because of its potential to act as a diagnostic for inflammatory diseases. Activated macrophages and neutrophils are a major source of hydrogen peroxide in inflammatory diseases[28,29]. We investigated the potential of peroxalate nanoparticles to image hydrogen peroxide, generated by activated macrophages and neutrophils, in a lipopolysaccharide (LPS) model of acute inflammation[30].

Mice were given an intraperitoneal injection of LPS, and 4 h later peroxalate nanoparticles containing pentacene were also injected into the peritoneal cavity, and imaged in an IVIS imaging system. Figure 4 shows that mice treated with LPS and peroxalate nanoparticles generated a greater intensity of chemiluminescence than mice treated with saline and peroxalate nanoparticles, demonstrating that the peroxalate nanoparticles can image the production of hydrogen peroxide *in vivo*.

For example, Fig. 4a shows a representative image of chemiluminescence emitted from mice treated with LPS and peroxalate nanoparticles versus mice treated with saline and peroxalate nanoparticles. Mice treated with LPS and peroxalate nanoparticles had a peak emission intensity of

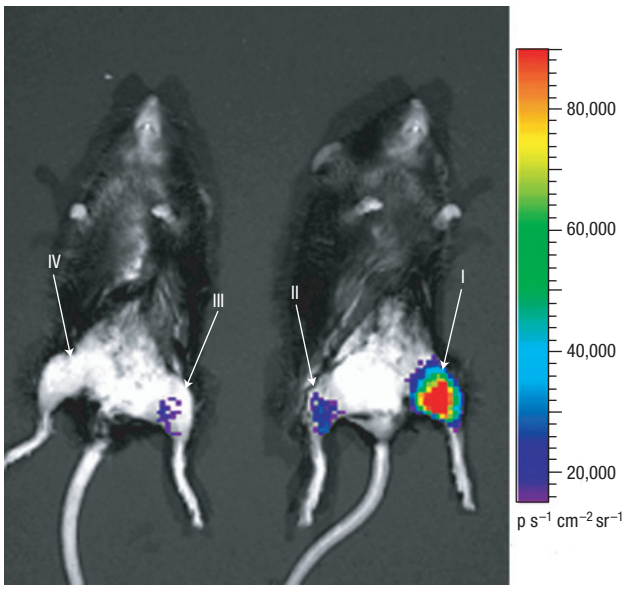

Figure 3 *In vivo* imaging of exogenous hydrogen peroxide using peroxalate nanoparticles. Peroxalate nanoparticles were mixed with various concentrations of hydrogen peroxide and injected, intramuscularly, into the leg, and then imaged in an IVIS imaging system. (I) Peroxalate nanoparticles + 10 μM of hydrogen peroxide; (II) peroxalate nanoparticles + 1 μM of hydrogen peroxide; (III) peroxalate nanoparticles only; (IV) negative control.

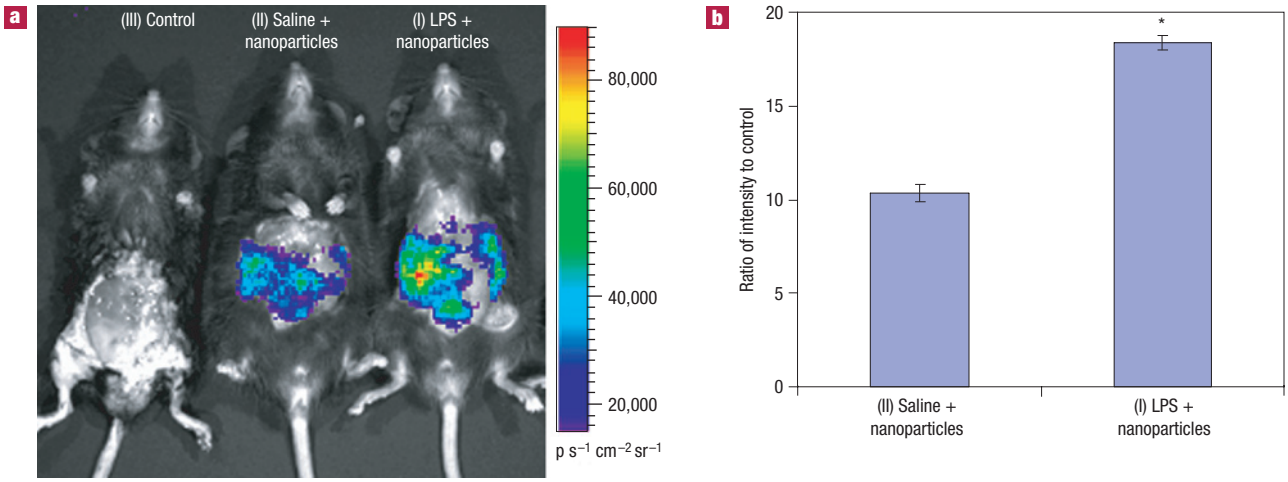

Figure 4 ***In vivo*** **imaging of endogenous hydrogen peroxide in the peritoneal cavity of mice, during an LPS-induced inflammatory response, using peroxalate nanoparticles. a**, (I) LPS was injected into the peritoneal cavity of mice, followed by an intraperitoneal injection of peroxalate nanoparticles 4 h later. (II) Saline was injected into the peritoneal cavity of mice, followed by an intraperitoneal injection of peroxalate nanoparticles 4 h later. (III) The negative control (no particles, no LPS). All images were taken 1 min after injection of the peroxalate nanoparticles and are a representative result of four experiments. **b**, Quantification of chemiluminescence emission intensity from groups (I)–(III) (in **a**). The total number of photons from the entire peritoneal cavity of groups (I)–(III) was integrated and plotted as a ratio to the control group, mean ± S.E, $n = 4$, $^{*}P < 0.01$ relative to group (II).

80,000 p s^{-1} cm^{-2} sr^{-1} from the peritoneal cavity, with a large fraction emitting from 40,000 to 60,000 p s^{-1} cm^{-2} sr^{-1}; in contrast, mice treated with saline and peroxalate nanoparticles had a peak emission intensity of only 40,000 p s^{-1} cm^{-2} sr^{-1}, and the majority of emission intensity was 20,000 p s^{-1} cm^{-2} sr^{-1} or below. To further quantify these results, the total number of photons emitted from the entire peritoneal cavity was integrated from each of the experimental groups and divided by the control group. Figure 4b demonstrates that mice treated with LPS and peroxalate nanoparticles generated almost two times higher chemiluminescence intensity than mice treated with saline and peroxalate nanoparticles. Taken together, these results suggest that peroxalate nanoparticles have the potential for imaging hydrogen peroxide-associated inflammatory diseases.

In summary, we have demonstrated that peroxalate nanoparticles can image hydrogen peroxide *in vivo* with high specificity and sensitivity. Peroxalate nanoparticles have great potential for imaging of hydrogen peroxide-associated diseases, given their high specificity and sensitivity and deep-tissue-imaging capability.

METHODS

SYNTHESIS OF POLYMER **1**

4-Hydroxybenzyl alcohol (16 mmol) and 1,8-octanediol (2.4 mmol) were dissolved in dry tetrahydrofuran (10 ml), under nitrogen, to which triethylamine (40 mmol) was added dropwise at 0 °C. This mixture was added to oxalyl chloride (18.3 mmol) in dry tetrahydrofuran (20 ml) at 0 °C. The reaction was kept at room temperature overnight, quenched with a saturated brine solution, and extracted with ethylacetate. The combined organic layers were dried over anhydrous Na_2SO_4 and concentrated under vacuum. The polymer **1** was isolated by precipitating in dichloromethane/hexane (1:1). The molecular weight was determined to be 8,900 (polydispersity = 2.6) by gel permeation chromatography using polystyrene standards. ^{1}H-NMR in deuterated chloroform on a 500 MHz spectrometer (Bruker): 7.5–7.4 (m, 2H, **Ar**), 7.3–7.2 (m, 2H, **Ar**), 5.4–5.3 (m, 2H, O**C**H_2–PhO), 4.4–4.2 (m, 4H, COO**C**$H_2$$CH_2$), 1.84–1.67 (m, 4H, OCH_2**C**H_2), 1.49–1.16 (m, 8H, OCH_2CH_2**C**H_2**C**H_2**C**H_2**C**$H_2$$CH_2CH_2O$).

NANOPARTICLE PREPARATION

Polymer (20 mg) was dissolved in 1.5 ml of dichloromethane, to which the fluorescent dye (1 mg) in 200 µl of dichloromethane was added. The mixture was added to 8 ml of a polyvinyl alcohol solution (5.0% in phosphate buffer pH 7.4) and homogenized, using a sonicator (Branson Sonifier 250) and homogenizer (Power Gen 500, Fisher Scientific), to form a fine oil/water emulsion. A nanoparticle suspension was prepared by rotary evaporation of dichloromethane for 30 min.

MEASUREMENT OF CHEMILUMINESCENCE

Peroxalate nanoparticles were diluted in sodium phosphate buffer (pH 7.4, 0.1 M) to give a concentration of 1 mg ml^{-1}. Various amounts of a hydrogen peroxide solution (1 mM in phosphate buffer pH 7.4, 0.1 M) were added to the nanoparticle suspensions, and the chemiluminescence was measured with a luminometer (Femtomaster FB12, Zylux Corporation) with a 10 s acquisition time. The chemiluminescence emission spectra were obtained using a spectrofluorometer (RF-5301-PC, Shimadzu).

IN VIVO IMAGING

C57Bl/6 mice, aged 8–10 weeks, were obtained from Jackson Labs. Pentacene-loaded nanoparticles (1 mg ml^{-1} in 0.1 M sodium phosphate buffer, pH 7.4) were mixed with either 1 or 10 µl of a 1 mM hydrogen peroxide solution (pH 7.4), and 200 µl of the nanoparticle suspension was injected intramuscularly into the legs of anaesthetized mice (ketamine/xylazine). Chemiluminescence images were captured with a 1 min acquisition time using an IVIS imaging system (Xenogen, USA).

For imaging of hydrogen peroxide generated in response to LPS-induced inflammation, 1 ml of LPS (1 mg ml^{-1} in saline) was injected into the peritoneal cavity of mice ($n = 4$) 4 h before the hydrogen peroxide imaging. Mice were anaesthetized with ketamine/xylazine and the hair and skin on the ventral surface of the abdomen was removed. One millilitre of pentacene-encapsulated peroxalate nanoparticles (1.5 mg ml^{-1} in sodium phosphate buffer, pH 7.4) was given to the mice intraperitoneally. Chemiluminescence images were captured with a 1 min acquisition time using an IVIS imaging system (Xenogen, USA).

Received 1 May 2007; accepted 17 July 2007; published 19 August 2007.

References

1. Lim, S. D. *et al.* Increased Nox1 and hydrogen peroxide in prostate cancer. *Prostate* **62**, 200–207 (2005).
2. Chang, M. C. Y., Pralle, A., Isacoff, E. Y. & Chang, C. J. A selective, cell-permeable optical probe for hydrogen peroxide in living cells. *J. Am. Chem. Soc.* **126**, 15392–15393 (2004).

3. Miller, E. W., Albers, A. E., Pralle, A., Isacoff, E. Y. & Chang, C. J. Boronate-based fluorescent probes for imaging cellular hydrogen peroxide. *J. Am. Chem. Soc.* **127**, 16652–16659 (2005).
4. Albers, A. E., Okreglak, V. S. & Chang, C. J. A FRET-based approach to ratiometric fluorescence detection of hydrogen peroxide. *J. Am. Chem. Soc.* **128**, 9640–9641 (2006).
5. Wu, M., Lin, Z. H., Schaferling, M., Durkop, A. & Wolfbeis, O. S. Fluorescence imaging of the activity of glucose oxidase using a hydrogen-peroxide-sensitive europium probe. *Anal. Biochem.* **340**, 66–73 (2005).
6. Wolfbeis, O. S., Schaferling, M. & Durkop, A. Reversible optical sensor membrane for hydrogen peroxide using an immobilized fluorescent probe, and its application to a glucose biosensor. *Microchim. Acta* **143**, 221–227 (2003).
7. Soh, N. Recent advances in fluorescent probes for the detection of reactive oxygen species. *Anal. Bioanal. Chem.* **386**, 532–543 (2006).
8. Troy, T., Jekic-McMullen, D., Sambucetti, L. & Rice, B. Quantitative comparison of the sensitivity fo detection of fluorescent and bioluminescent reporters in animal models. *Mol. Imag.* **3**, 9–23 (2004).
9. Rice, B. W., Cable, M. D. & Nelson, M. B. *In vivo* imaging of light-emitting probes. *J. Biomed. Opt.* **6**, 432–440 (2001).
10. Chen, W.-T. & Ralph Weissleder, C.-H. T. Imaging reactive oxygen species in arthritis. *Mol. Imag.* **3**, 159–162 (2004).
11. Hosaka, S., Itagaki, T. & Kuramitsu, Y. Selectivity and sensitivity in the measurement of reactive oxygen species (ROS) using chemiluminescent microspheres prepared by the binding of acridinium ester or ABEI to polymer microspheres. *Luminescence* **14**, 349–354 (1999).
12. Rauhut, M. M., Roberts, B. G., Maulding, D. R., Bergmark, W. & Coleman, R. Infrared liquid-phase chemiluminescence from reactions of bis(2,4,6-trichlorophenyl) oxalate, hydrogen-peroxide, and infrared fluorescent compounds. *J. Org. Chem.* **40**, 330–335 (1975).
13. Arnous, A., Petrakis, C., Makris, D. P. & Kefalas, P. A peroxyoxalate chemiluminescence-based assay for the evaluation of hydrogen peroxide scavenging activity employing 9,10-diphenylanthracene as the fluorophore. *J. Pharm. Toxicol. Methods* **48**, 171–177 (2002).
14. Hadd, A. G., Lehmpuhl, D. W., Kuck, L. R. & Birks, J. W. Chemiluminescence demonstration illustrating principles of ester hydrolysis reactions. *J. Chem. Educ.* **76**, 1237–1240 (1999).
15. Motoyoshiya, J. *et al.* Peroxyoxalate chemiluminescence of N,N′-bistosyl-1H,4H-quinoxaline-2,3-dione and related compounds. Dependence on electronic nature of fluorophores. *J. Org. Chem.* **67**, 7314–7318 (2002).
16. Gubitz, G., Vanzoonen, P., Gooijer, C., Velthorst, N. H. & Frei, R. W. Immobilized fluorophores in dynamic chemi-luminescence detection of hydrogen-peroxide. *Anal. Chem.* **57**, 2071–2074 (1985).
17. Koike, R., Kato, Y., Motoyoshiya, J., Nishii, Y. & Aoyama, H. Unprecedented chemiluminescence behaviour during peroxyoxalate chemiluminescence of oxalates with fluorescent or electron-donating aryloxy groups. *Luminescence* **21**, 164–173 (2006).
18. Tsunoda, M. & Imai, K. Analytical applications of peroxyoxalate chemiluminescence. *Anal. Chim. Acta* **541**, 13–23 (2005).
19. Stevani, C. V., Silva, S. M. & Baader, W. J. Studies on the mechanism of the excitation step in peroxyoxalate chemiluminescence. *Eur. J. Org. Chem.* 4037–4046 (2000).
20. Matsumoto, M. Advanced chemistry of dioxetane-based chemiluminescent substrates originating from bioluminescence. *J. Photochem. Photobiol. C* **5**, 27–53 (2004).
21. Schuster, G. B. Chemi-luminescence of organic peroxides—conversion of ground-state reactants to excited-state products by the chemically-initiated electron-exchange luminescence mechanism. *Acc. Chem. Res.* **12**, 366–373 (1979).
22. Hilderbrand, S. A., Kelly, K. A., Weissleder, R. & Tung, C. H. Monofunctional near-infrared fluorochromes for imaging applications. *Bioconjug. Chem.* **16**, 1275–1281 (2005).
23. Polytarchou, C., Hatziapostolou, M. & Papadimitriou, E. Hydrogen peroxide stimulates proliferation and migration of human prostate cancer cells through activation of activator protein-1 and up-regulation of the heparin affin regulatory peptide gene. *J. Biol. Chem.* **280**, 40428–40435 (2005).
24. Laurent, A. *et al.* Controlling tumor growth by modulating endogenous production of reactive oxygen species. *Cancer Res.* **65**, 948–956 (2005).
25. Stone, J. R. & Collins, T. The role of hydrogen peroxide in endothelial proliferative responses. *Endothelium-New York* **9**, 231–238 (2002).
26. Mohler, D. L. & Shell, T. A. The hydrogen peroxide induced enhancement of DNA cleavage in the ambient light photolysis of CpFe(CO)(2)Ph: A potential strategy for targeting cancer cells. *Bioorg. Med. Chem. Lett.* **15**, 4585–4588 (2005).
27. Hirpara, J. L., Clement, M. V. & Pervaiz, S. Intracellular acidification triggered by mitochondrial-derived hydrogen peroxide is an effector mechanism for drug-induced apoptosis in tumor cells. *J. Biol. Chem.* **276**, 514–521 (2001).
28. Sredni-Kenigsbuch, D., Kambayashi, T. & Strassmann, G. Neutrophils augment the release of TNF alpha from LPS-stimulated macrophages via hydrogen peroxide. *Immunol. Lett.* **71**, 97–102 (2000).
29. Hikosaka, K. *et al.* Reduced lipopolysaccharide (LPS)-induced nitric oxide production in peritoneal macrophages and inhibited LPS-induced lethal shock in mice by a sugar cane (*Saccharum officinarum* L.) extract. *Biosci. Biotechnol. Biochem.* **70**, 2853–2858 (2006).
30. Chen, W. T., Mahmood, U., Weissleder, R. & Tung, C. H. Arthritis imaging using a near-infrared fluorescence folate-targeted probe. *Arthritis Res. Ther.* **7**, R310–R317 (2005).

Acknowledgements

This work was supported by the Georgia Tech/Emory Center for the Engineering of Living Tissues (funded by NSF-EEC-9731643) (N.M.), NSF-BES-0546962 Career Award (N.M.), NIH UO1 HL80711-01 (N.M.), NIH R21 EB006418 (N.M.), J&J/GT Health Care Innovation Seed Grant Proposal (N.M.) and NIH P01 HL58000 (W.R.T.). The authors would like to thank R. Dasari (Department of Chemistry, Georgia Institute of Technology) for nuclear magnetic resonance and Fourier transform infrared analysis.
Correspondence and requests for materials should be addressed to N.M.
Supplementary Information accompanies this paper on www.nature.com/naturematerials.

Competing financial interests

The authors declare no competing financial interests.